Finite element analysis of ultrasonic CFRP laminate inspection

Jeff Dobson, Anthony Gachagan and Richard O'Leary
Centre for Ultrasonic Engineering, University of Strathclyde
Glasgow, G1 1RD, UK
jeff.dobson@strath.ac.uk

Andrew Tweedie and Gerald Harvey
PZFlex, Thornton Tomasetti
Glasgow, G1 2ER, UK

Abstract

Carbon Fibre Reinforced Polymer (CFRP) materials pose a challenge for NDE inspections due to their anisotropic material properties and often complex morphologies. Simulation is a vital tool in the design of ultrasonic inspections, improving setup and helping understand wave propagation in complex components. In this work, three different approaches of constructing accurate Finite Element Analysis (FEA) models of CFRP components are presented. The first approach generates a model of a flat CFRP laminate using the design specification to construct the idealised laminate geometry – essentially recreating the 'as designed' component in the model. The second approach utilises photomicrographs of the laminates' cross-section to produce a more realistic 'as built' geometry within the model. Ultrasonic inspection simulations performed show a good correlation when comparing resulting A-scans with experiments. A final modelling approach of using an image of X-Ray CT data is then performed to develop an accurate model of a tapered composite structure. This paper presents the construction of the finite element models using PZFlex and the subsequent results highlighting the ability of the simulations to recreate experimental inspection performance.

1. Introduction

Over the last decade there has been a rapid increase in the use of composite materials in many engineering components. This is due to their ability to provide increased mechanical strength while also yielding weight savings in structures. With the use of composite materials expanding into more wide-ranging fields, the requirement for advanced research into composite inspections also increases. Composite materials pose a difficult challenge to inspect due to their anisotropy and in many cases complex component geometries. Thus, the need for advanced Non-Destructive Evaluation (NDE) inspections becomes critical. Modelling is an essential tool for designing and evaluating these NDE inspections and allows for inspections to be optimised in a reduced time frame.

The overall objective of this research is to develop methods to generate accurate Finite Element Analysis (FEA) models of Carbon Fibre Reinforced Polymer (CFRP) components to allow for ultrasonic inspections to be simulated. Three main data sources

for constructing models from are highlighted as: component design specification, microscopy and X-Ray CT. The ability to construct models from any of these sources offers a wide versatility for model generation. This paper describes work carried out to create FEA models of CFRP components using all three data sources. Ultrasonic inspection simulations are performed using PZFlex software (Thornton Tomasetti, Cupertino, USA) and compared with experimental data.

2. Method

The test sample used for this work was a flat CFRP laminate, as shown in Figure 1(a). This laminate comprises woven 2/2 twill as both the top and bottom layers, while 23 unidirectional layers are sandwiched in between. The laminate was 100mm square and had an approximate thickness of 6.2 ± 0.1 mm.

2.1 Sample preparation work

In order to facilitate microscopy, a sample was cut from the CFRP plate, the exposed edges of the laminate was then manually polished using 1µm lapping powder. This produced a polished finish to the side of the sample allowing for high magnification microscopic images to be taken, as seen in Figure 1(b). Individual photomicrograph images were then stitched together to produce an image of the cross section of the sample, as shown in Figure 1(c). The number of plies, ply layup, ply thickness, twill thickness and resin thickness could then be determined from these images.

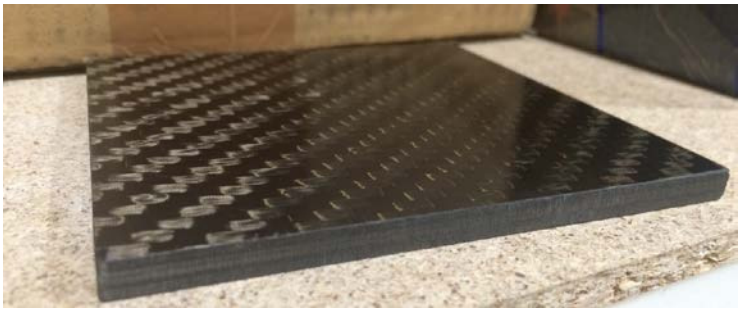

(a)

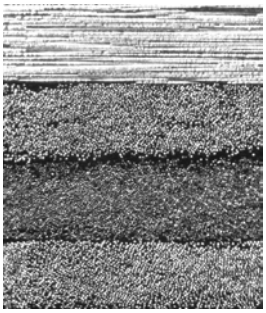

(b)

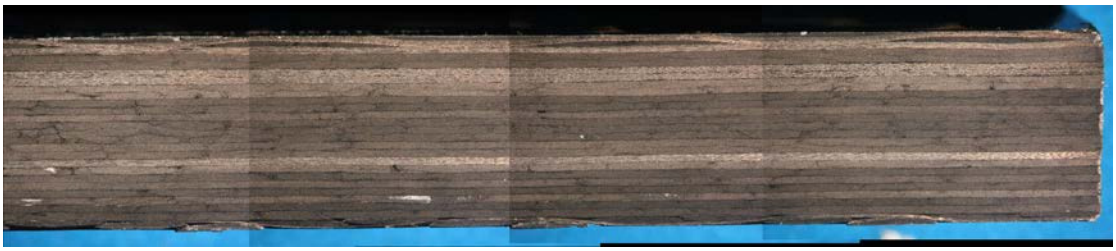

(c)

Figure 1. (a) Photograph of CFRP laminate sample, (b) high magnification microscopic image of sample showing (top to bottom) 90°, 45°, 0° and 45° unidirectional layers and (c) photomicrograph of sample cross-section

2.2 Experimental configuration

An immersion pulse-echo inspection was conducted to collect experimental A-scans to provide a comparison for simulation results. An Olympus 5MHz single element immersion transducer was used and was driven by a 100ns pulse. The transducer was circular with a diameter of 19mm. The sample was submerged in water and supported at each end using plastic stands to ensure no interference at the back wall was observed. The transducer was manually positioned 3mm from the surface of the sample, as illustrated in Figure 2. An oscilloscope was then used to view and acquire the resulting A-scan signals from the pulse-echo inspections on the CFRP sample. This process was repeated several times at different locations across the sample surface.

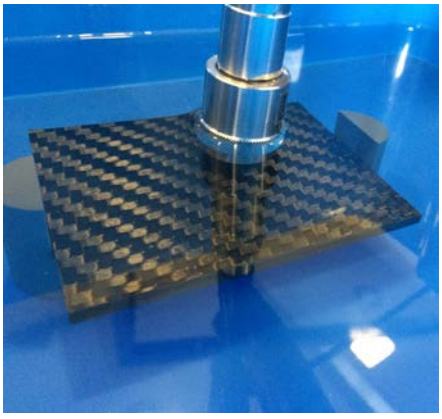

Figure 2. Photograph of experimental configuration

2.3 Simulation model development

Accurate finite element models are heavily dependent on the ability to recreate the material geometry and material properties. CFRP provides challenges in both geometry and material properties due to component geometry structure and anisotropic properties of the layers within the component.

To generate the geometry of the test sample, two different approaches were utilised. The first used design specifications to produce an idealised geometry. The second utilised the micrographic images to build the model geometry to give a more representative model. The material properties used in the PZFlex models for water, resin and CFRP can be seen in Table 1, Table 2 and Table 3 respectively. The CFRP anisotropic material properties were transformed to local coordinate systems relating to the orientation of the CFRP ply layers. Accurate material damping data was not available for the resin or CFRP and was not included in the models used in this work.

Table 1. Water material properties [(1)]

Density (kgm^{-3})	Longitudinal Velocity (ms^{-1})	Shear Velocity (ms^{-1})	Longitudinal attenuation (dB/m)	Shear attenuation (dB/m)
1000	1496	0	0.002	0

Table 2. Resin material properties [2]

Density (kgm^{-3})	Young's Modulus (GPa)	Poisson's ratio
1310	3.32	0.35

Table 3. CFRP material properties [3]

Density (kgm^{-3})	E_{11} (GPa)	$E_{22} = E_{33}$ (GPa)	$G_{12} = G_{13}$ (GPa)	G_{23} (GPa)	$\upsilon_{12} = \upsilon_{13}$	υ_{23}
1620	153	10.3	5.2	3.43	0.3	0.5

A signal received by the transducer when reflected off a glass sample was recorded. This would provide a reference signal that could be used in the PZFlex model to represent the transducer as a pressure load. The reference signal and its frequency spectrum can be seen in Figure 3. The transducer used in the work is a commercial device and so the approach taken removes the requirement for knowledge of the internal transducer structure. Removing the electro-mechanical calculation from the simulation also means it is more computationally efficient. The average pressure in the model elements across the aperture of the transducer were recorded to produce the resulting A-scan signals.

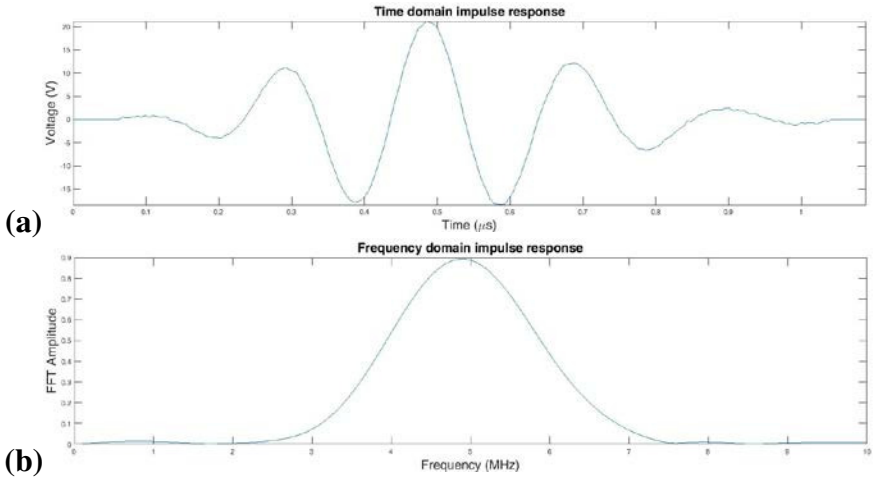

Figure 3. Experimental (a) time and (b) frequency domain impulse response of the 5MHz transducer used as model reference signal

2.3.1 Design specifications

To create the ideal laminate geometry the layer thickness and twill dimensions were measured from the micrograph. The twill dimensions were used in TexGen software (University of Nottingham, UK) [4] to construct a 2/2 twill woven textile, as shown in Figure 4. This was then reduced to a 2D cross section and exported as a voxel file which was then converted into a native PZFlex geometry format to allow for easy importation into the modelling suite.

The PZFlex model was constructed to read in the twill table file twice for the top and bottom layers, while the unidirectional layers and resin layers were hard coded. The

orientation of the unidirectional layers were determined from the micrograph of the laminate surface. However, using this method it is not possible to tell if the 45° fibres are in plus or minus direction, so all are assumed in the plus direction. The sample was modelled immersed in a water load and a dummy material was introduced to represent the transducer. This would also provide the source for the pressure load to apply the drive function into the model. The resulting CFRP laminate geometry created in PZFlex can be seen in Figure 5 where each colour represents a different ply orientation.

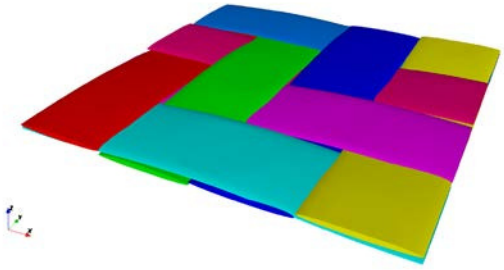

Figure 4. 2/2 twill textile created in TexGen

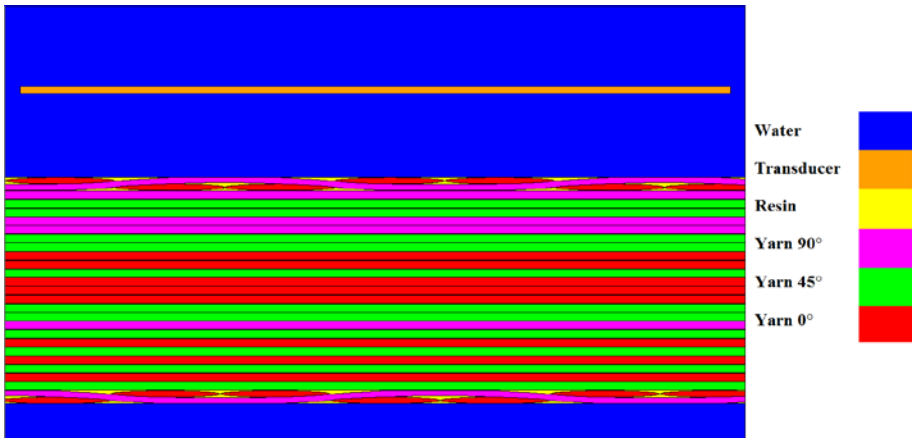

Figure 5. PZFlex model geometry for sample design specification geometry

The 2/2 twill woven layers had a thickness of 360µm, ply layers had a thickness of 230µm and the intermediate resin layers were 10µm thick. This gave an overall sample thickness of 6.25mm. The model element size was determined by the thin resin layers, where a minimum of three elements through the thickness was used to capture stress gradients. Therefore the size of the individual elements was set to be a third of the resin layer thickness. This achieves an appropriate balance between computational efficiency and model accuracy. This produced a model containing approximately 21 million elements which when run on a workstation with 64 GB of RAM and 16 hyper threaded cores took 2 hours to run. It should be noted that to help reduce the number of elements required and the computation costs, it is possible to alter the element aspect ratio, and to have different mesh sizes throughout the model.

2.3.2 Micrograph image processing

To increase the accuracy of the PZFlex model of the CFRP, the photomicrograph image, shown in Figure 1(c), was used to generate a TexGen textile of the 23 unidirectional layers. This approach accounts for the ply waviness and variation in resin

thickness observed in the 'as built' composite structure. This textile was then used to construct a PZFlex model of the laminate incorporating the previously created twill for the top and bottom layers. The overall thickness of the sample in this model was 6.22mm and the model had a similar number of elements and run time as the model described in Section 2.3.1. A section of the resultant material map of the PZFlex model is compared to the previous design specification model in Figure 6. This highlights the difference of how the CFRP layers are represented in the respective modelling approaches.

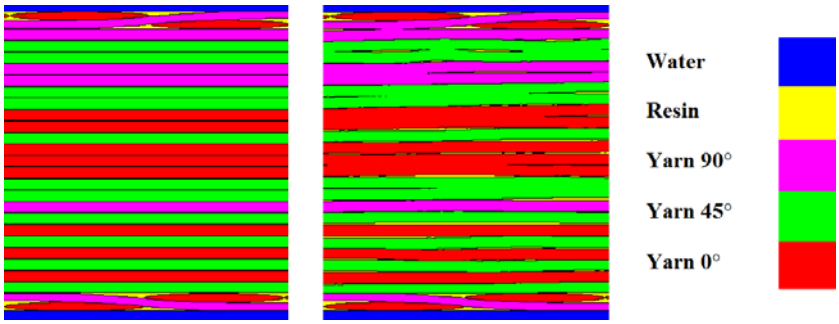

Figure 6. Comparison of PZFlex model geometry for (left) design specification geometry and (right) actual sample geometry

3. Results and discussion

The recorded A-scan time traces from the experiment and simulations were cropped to show the front wall and back wall reflections. In each result, the response due to the ply layers and resin can clearly be seen between the front wall and back wall reflections. Example A-scan results can be seen in Figure 7 for the experimental, ideal geometry simulation and actual geometry simulation. Figure 8 plots the A-scans with the Hilbert function applied to allow for the time between front wall and back wall reflections to be measured.

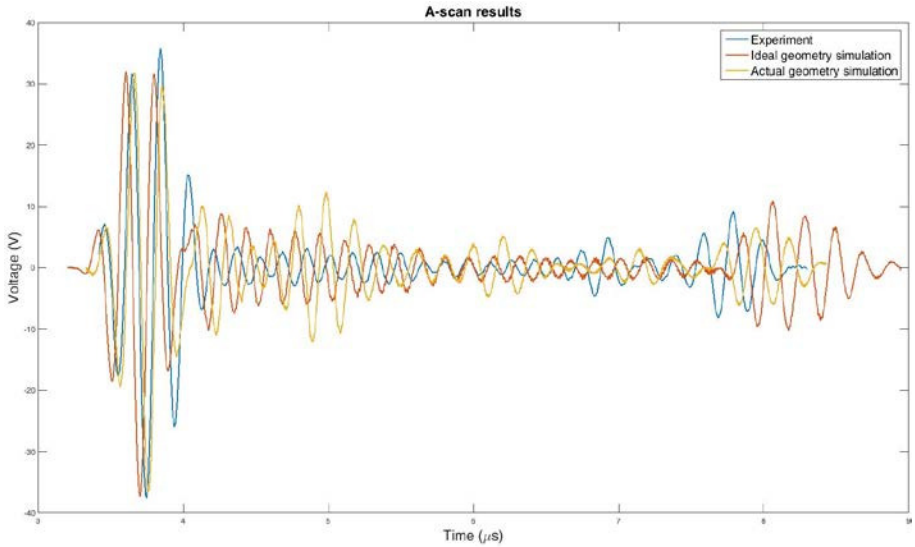

Figure 7. A-scan results for experiment, ideal geometry simulation and actual geometry simulation

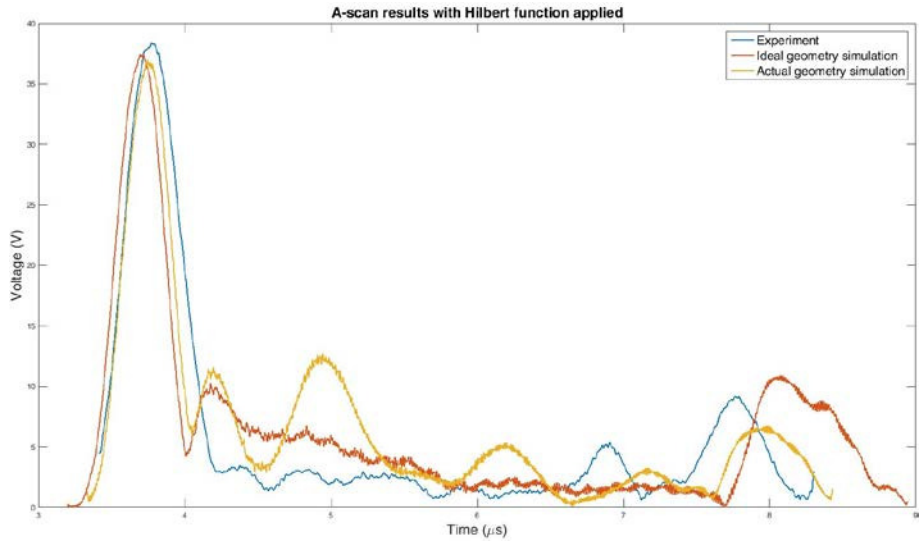

Figure 8. A-scan results with Hilbert function applied for experiment, ideal geometry simulation and actual geometry simulation

To provide a comparison between the experiment and simulation results, the time between the front wall and back wall peaks was investigated. Using the plots of the A-scans with the Hilbert function applied, the time difference between the front wall and back wall signal peaks was measured. Table 4 shows the measured time of flights for the experiments (sorted in order from slowest to fastest) and Table 5 contains the average experimental time along with the two simulations.

Table 4. A-scan time of flights between front wall and back wall reflections

Experiment A-scan number	1	2	3	4	5	6
Time (μs)	3.948	3.958	3.969	3.979	3.989	4.021

Table 5. A-scan time of flights between front wall and back wall reflections

	Experiment Average	Ideal geometry simulation	Actual geometry simulation
Time (μs)	3.977	4.367	4.233

The simulations have predicted the shape and characteristics of the experimental A-scan well. However, there is some error in the time of flight between the front wall and back wall reflections. There are several approximations within the model which can explain the reasoning for these errors.

The main source for error in the model is the uncertainty of the material properties. The material properties play a significant role in determining the sound velocity through a material and therefore the propagation time associated with this scenario.

The overall thickness of a composite can exhibit variability along its major dimensions. This will mean the time of flight through the thickness will have some uncertainty as

seen in the different times measured for each experimental A-scan. The simulations have been set up as accurately as possible but is still an approximation as the modelled cross-section will differ slightly from the cross-section of the composite where the experimental A-scan was collected.

A final difference between simulation and experiment is the approximation to a two dimensional simulation. The real world experiment is naturally a three dimensional problem but for computational efficiency, this was reduced to a 2D plane strain model.

To demonstrate the simulations are predicting experimental characteristics, despite uncertainties in material properties, the frequency components of the A-scans were investigated. The time traces were split into three sections: front wall reflection, resin reflections and back wall reflection - the FFT was used to determine the spectral content of each A-scan section. The results can be seen in Figures 9, 10 and 11. These figures plot both the time domain signals and their frequency spectrum.

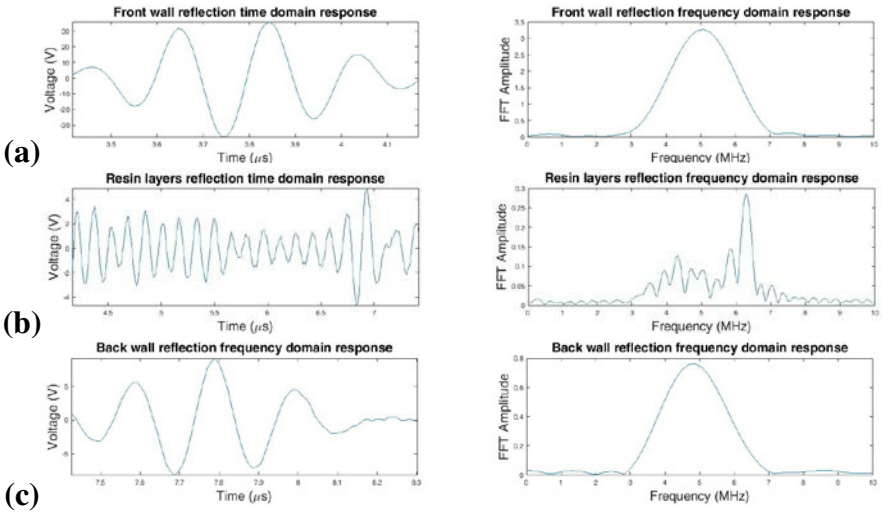

Figure 9. Time and frequency domain response for experiment A-scan (a) front wall reflection, (b) resin reflections and (c) back wall reflection

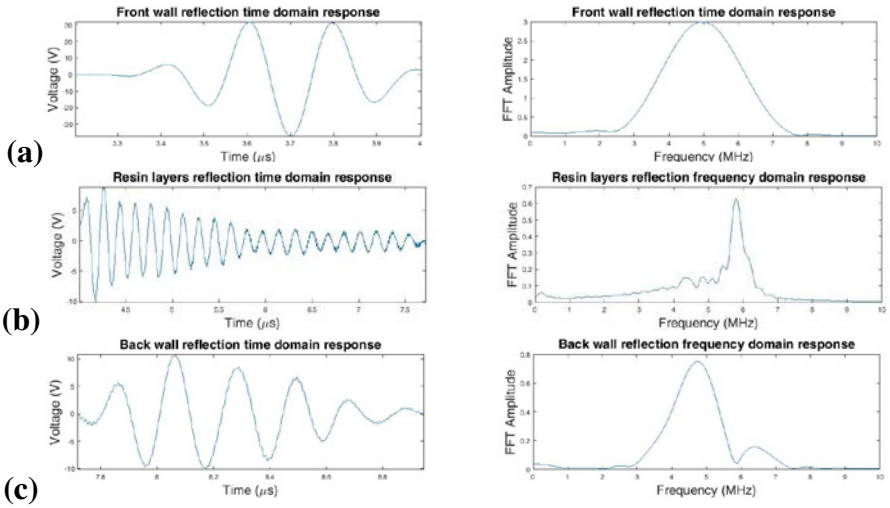

Figure 10. Time and frequency domain response for ideal geometry simulation A-scan (a) front wall reflection, (b) resin reflections and (c) back wall reflection

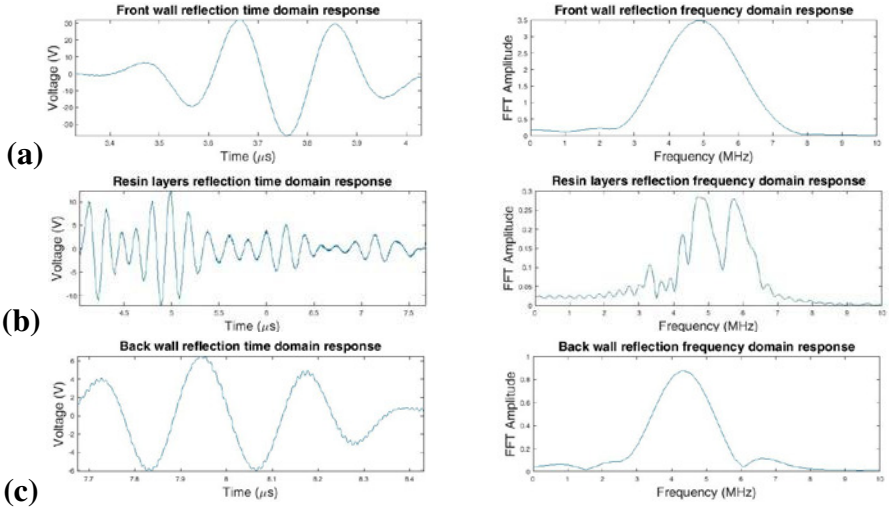

Figure 11. Time and frequency domain response for actual geometry simulation A-scan (a) front wall reflection, (b) resin reflections and (c) back wall reflection

It can be seen that when comparing the individual frequency components of the A-scans, there are similarities between simulation and experiment. In all three cases the frequency content of the front wall reflection matches the drive signal frequency content as would be expected. For the back wall reflection frequency content, the actual geometry simulation best matches the experiment. The ideal geometry simulation differs as the perfect layers cause the signal to be filtered more in the higher frequency range and hence, it has a longer ring down.

The resin reflections contain higher frequency content which is related to the resonance of the layers. The peak of the resin layer frequency in the simulations is slightly less than the experiment which is due to uncertainty in material properties. There is a peak at 5MHz in the actual geometry simulation which indicates a strong reflection from a thick resin layer. This was also seen when a different experimental A-scan was inspected, as shown in Figure 12. In the experiment this could also be a reflection from a thick resin layer or it could also indicate a reflection from a delamination defect.

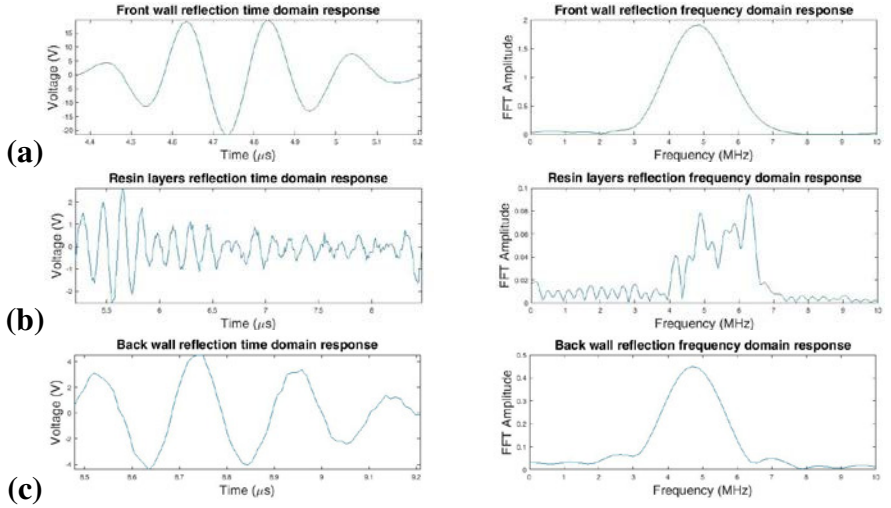

Figure 12. Time and frequency domain response for second experiment location A-scan (a) front wall reflection, (b) resin reflections and (c) back wall reflection

4. Complex structure

Composites offer the ability to tailor the structural geometry and save weight by tapering the structure thickness. This is achieved by terminating individual plies at discrete locations known as ply drops as illustrated in Figure 13 [5]. These structures are difficult to inspect due to the presence of angled plies in the component structure. These angled plies have a big impact on the wave propagation and greatly distort the ultrasonic signal.

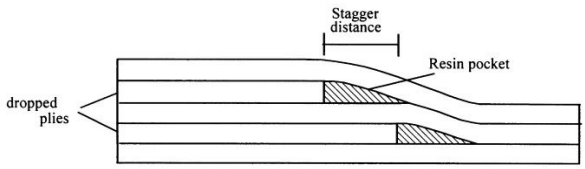

Figure 13. Illustration of a ply drop in a composite sample [5]

To demonstrate the capability of PZFlex at modelling these complex composite structures, the modelling approach was extended to simulate an inspection of a tapered composite. A cross sectional image of X-Ray CT data of a tapered composite structure was used to generate a PZFlex model, as seen in Figure 14 and Figure 15 respectively. The X-Ray CT dataset was obtained using a source voltage of 49kV and produced an 8-bit Tiff stack with a pixel size of 19.5µm. A TexGen textile was constructed of the tapered composite and the voxel and orientation files were exported. A PZFlex material map was then generated to represent the tapered composite geometry while also creating multiple material instances for each individual ply layer representing different orientation angles in the Z-Axis. This is a key element for these types of models as the different angles of plies play a significant role on the wave propagation and interaction at their boundaries.

Figure 14. Cross sectional image of tapered composite sample. Image courtesy of University of Bristol

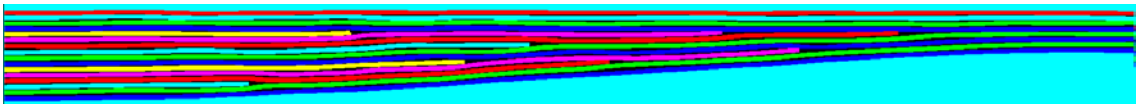

Figure 15. Tapered composite PZFlex model geometry

A good visual and qualitative correlation between the actual structure geometry and PZFlex model geometry was obtained, as illustrated in Figure 16, where the PZFlex model geometry is overlaid the X-Ray CT data image.

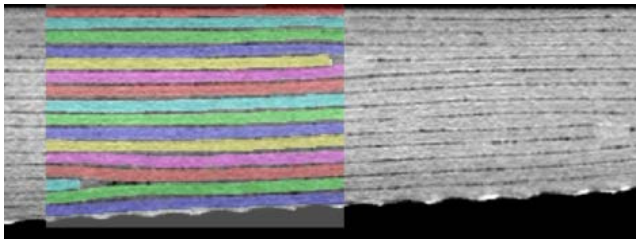

Figure 16. Section of PZFlex model overlaid on image of tapered composite X-Ray CT data.

An immersion inspection of the tapered composite was simulated in PZFlex and the predicted Hilbert transformed B-scan is shown in Figure 17. In order to extract further detail from the FEA derived dataset, individual A-scans can be seen in Figure 18 for 5mm, 20mm and 30mm along the horizontal of the tapered sample, where 0mm is at the thickest section of the composite, as seen in Figure 17.

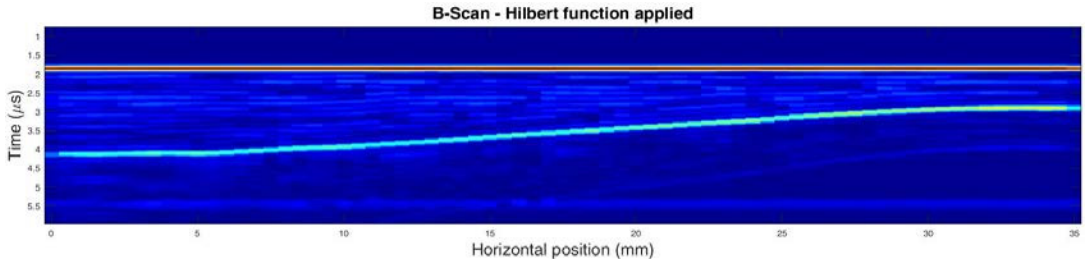

Figure 17. B-scan of tapered composite with Hilbert function applied

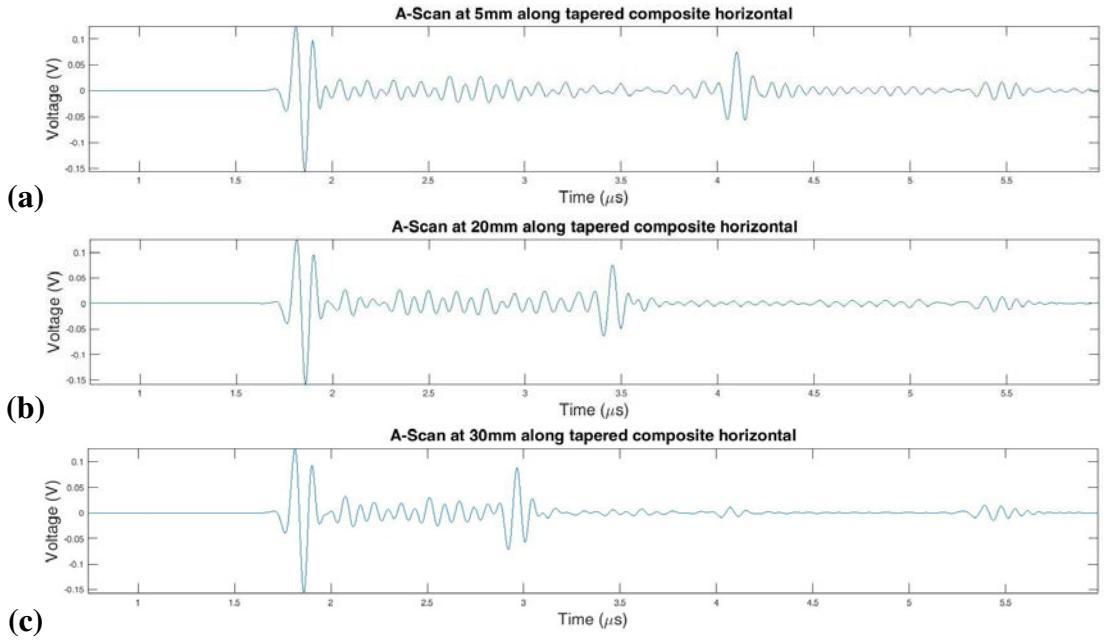

Figure 18. A-scans of tapered composite inspection at (a) 5mm, (b) 20mm, and (c) 30mm along the horizontal position of the tapered sample, where 0mm is at the thickest section

These predicted A-scans are similar to results presented in Section 3 for the flat laminate. There are clear front wall and back wall reflections either side of reflections from the resin layers. It is very easy to see the changing thickness of the tapered

composite structure from the B-scan. Interestingly, although not fully explored at this stage in the research, indications of ply drops are evident in Figure 17 and with further post processing, could be easily identified.

5. Conclusions and future work

This paper has described work conducted to produce FEA models of CFRP laminates for the simulation of ultrasonic inspections. Three different data sources, design specification, photomicrograph and X-Ray CT, have been used to construct model geometries. It has been shown that FEA can provide the ability to simulate ultrasonic inspections of CFRP laminates. This will provide great benefit in allowing NDE inspections of composite components to be designed and evaluated through simulations.

The future work of this research will look to improve the model generation and improve model efficiency. This will allow for models to be created and executed in a computationally efficient manner, while also creating the opportunity for large 3D models to be implemented. Focussing on the generation of PZFlex models from micrograph or X-Ray CT images is prudent as they provide the most representative model geometry construction. This includes extending the image processing techniques described here, for rapid and facile generation of models. This will open up the possibility to read in multiple images from X-Ray CT data to generate a full 3D PZFlex model. The research will also look into novel meshing approaches to ensure model accuracy and reduce computation costs.

Acknowledgements

Funding from the Engineering and Physical Sciences Research Council for an Engineering Doctorate studentship is gratefully acknowledged (Grant no. EP/I017704/1), as is financial, technical and practical support by Thornton Tomasetti, the University of Strathclyde and the wider UK Research Centre in NDE. The authors would also like to thank Prof Smith and his team at the University of Bristol for generating the tapered composite sample image used in Section 4.

References

1. F Duck, ‘Physical properties of tisues: a comprehensive reference book’, Academic press, 2013.
2. A Case, ‘Permeability of hybrid composites subjected to extreme thermal cycling and low-velocity impacts, MS Thesis, Georgia Institute of Technology, 2004.
3. A Ataş, A Hodzic and C Soutis, ‘Strength prediction of bolted joints in cross-ply laminates based on subcritical damage modelling’, ECCM15 – 15th European conference on composite materials, Venice, Italy, 24-28 June 2012.
4. A Long and L Brown, ‘Modelling the geometry of textile reinforcements for composites: Texgen’, Composite reinforcements for optimum performance, Woodhead Publishing, pp 239-264, 2011.
5. A Mukherjee and B Varughese, ‘Design guidelines for ply drop-off in laminated composite structures’, Composites Part B: Engineering, vol. 32, no. 2, pp. 153-164, 2001.